## Title

GABA progenitors grafted into the adult epileptic brain control seizures and abnormal behavior.



## Journal

Nature Neuroscience, 16(6)

## Authors

Girskis, Kelly
Baraban, Scott
Rubenstein, John
et al.

## Publication Date

2013-06-01

## DOI

10.1038/nn.3392

Peer reviewed

HHS Public Access

Author manuscript

*Nat Neurosci*. Author manuscript; available in PMC 2013 December 01.

Published in final edited form as:

*Nat Neurosci*. 2013 June ; 16(6): 692–697. doi:10.1038/nn.3392.

# GABA progenitors grafted into the adult epileptic brain control seizures and abnormal behavior

**Robert F. Hunt**[1,2], **Kelly M. Girskis**[1,2], **John L. Rubenstein**[3], **Arturo Alvarez–Buylla**[2], and **Scott C. Baraban**[1,2]

[1]Epilepsy Research Laboratory, University of California, San Francisco

[2]Department of Neurological Surgery, University of California, San Francisco

[3]Department of Psychiatry, University of California, San Francisco

## Abstract

Impaired GABA–mediated neurotransmission has been implicated in many neurologic diseases including epilepsy, intellectual disability, and psychiatric disorders. Here we report that inhibitory neuron transplantation into the hippocampus of adult mice with confirmed epilepsy at the time of grafting dramatically reduced the occurrence of electrographic seizures and restored behavioral deficits in spatial learning, hyperactivity, and the aggressive response to handling. In the recipient brain, GABA progenitors migrated up to 1500 μm from the injection site, expressed genes and proteins characteristic for interneurons, differentiated into functional inhibitory neurons, and received excitatory synaptic input. In contrast to hippocampus, cell grafts into basolateral amygdala rescued the hyperactivity deficit but did not alter seizure activity or other abnormal behaviors. Our results highlight a critical role for interneurons in epilepsy and suggest that interneuron cell transplantation is a powerful approach to halt seizures and rescue accompanying deficits in severely epileptic mice.

## Introduction

GABA–producing inhibitory interneurons play essential roles in regulating cortical excitability and coordinating appropriate behaviors. In hippocampus, interneuron dysfunction has been implicated in many forms of epilepsy[1,2] and can disrupt learning and



Correspondence and requests for materials should be addressed to R.F.H. (Robert.Huntiii@ucsf.edu) or S.C.B (Scott.Baraban@ucsf.edu).

**Competing Financial Interests:**
S.C.B., J.L.R. and A.A-B. are cofounders of and have a financial interest in Neurona Therapeutics.

Supplementary Information is linked to the online version of the paper at www.nature.com/neuro.

**Author Information** Reprints and permissions information is available at www.nature.com/reprints. S.C.B., J.L.R. and A.A–B. are cofounders of and have a financial interest in Neurona Therapeutics.

**Author Contributions** R.F.H. contributed to the concept, design, execution and analysis of all experiments, funding, and wrote the manuscript. K.M.G. contributed to execution and analysis of the immunostaining and behavior experiments. J.L.R. and A.A.B. contributed to the concept, funding, and to manuscript editing. S.C.B. contributed to concept, design, analysis of EEG data, funding, and manuscript writing.

memory[3] or social behaviors[4]. Current medications that systemically potentiate GABA–mediated inhibition can be effective in suppressing seizures, but prolonged drug treatment can have unwanted cognitive or neurobehavioral side effects and epilepsy remains refractory to medical treatment in nearly one–third of affected individuals[5]. Recently, optogenetic techniques have been shown to interrupt seizure activity in animal models of epilepsy[6,7], supporting the general concept that focal inhibition of epileptic networks might have therapeutic application. Although promising, these approaches require expression of light–sensitive opsins, invasive light delivery interface, and seizure–detection hardware. Transplantation and subsequent integration of new inhibitory neurons into neural circuits affected by epilepsy might be a therapeutic strategy to control seizures, or other co–occurring behaviors, as a one–time procedure without need for regular neural modulation or online seizure prediction.

The majority of cortical interneurons are born in the medial ganglionic eminence (MGE) of the embryonic ventral telencephalon[8–11]. When grafted into the neonatal brain, MGE progenitor cells migrate long distances and functionally integrate as inhibitory neurons[9, 12–14]. In a previous study, we showed that early postnatal transplantation of GABA progenitor cells into neocortex, prior to seizure onset, reduced spontaneous electrographic seizure activity in mice with a congenital potassium channel mutation[13]. However, whether this approach would be successful in the more common and medically refractory types of epilepsy seen in adults has not been directly tested. The emergence of epilepsy in adulthood involves a wide range of modifications to brain structure and function[1,2], and it is not known whether the adult nervous system can support GABA progenitor cell migration, differentiation, integration, or functional recovery of pre–existing deficits.

On this basis, we first carefully characterized the development of MGE progenitors grafted into adult recipients. Then, we asked whether epileptic phenotypes could be improved by MGE cell grafts into hippocampus or amygdala after epileptic seizures emerge (Supplementary Fig. 1). For this purpose, we selected a pilocarpine model of epilepsy that is characterized by robust, frequent spontaneous seizures acquired after a brain insult[15–18], well–described behavioral abnormalities[18], and responds poorly to antiepileptic drugs[19]. These animals recapitulate several key features of human temporal lobe epilepsy, the most common type of epilepsy in adults[1,2].

## Results

MGE progenitors were obtained from E13.5 β–actin:GFP donor mice[20], as previously described[9,12–14], and $3 \times 10^4$ cells were injected into the dorsal hippocampus of adult (P60) control recipients. The migration (Fig. 1a) and neurochemical expression (Fig. 1b) of grafted cells was examined seven and 60 days after transplantation (DAT). By 7 DAT, MGE–GFP cells had moved away from the injection and dispersed throughout hippocampal subfields (n=3 animals; Supplementary Fig. 2). Many grafted cells were found along major fiber tracts and exhibited a bipolar, “migratory” morphology, while others started to extend multiple processes from the cell body. Survival rate at 7 DAT was 32.6 ± 2.3% (n=3). By 60 DAT (n=6 animals), these cells had migrated up to 1500 μm from the injection site, and survival

was 14.8 ± 1.3%. We did not detect a significant difference in the mean rostrocaudal distance of grafted MGE cells at 60 DAT compared to 7 DAT (Fig. 1a; P=0.44; two–tailed t-test), suggesting rostrocaudal migration is nearly complete by 7 DAT. At 60 DAT, most GFP–labeled cells had morphological features of mature interneurons with large, extensive processes and cell bodies positioned in regions normally occupied by endogenous inhibitory neurons (i.e., polymorph and molecular layers). GFP–labeled cells expressed NeuN (92.2 ± 2.9%), GAD67 (63 ± 4.4%), and interneuron markers, with somatostatin (SST; 41.3 ± 2.8%), neuronal nitric oxide synthase (nNOS; 21.6 ± 1.2%), and parvalbumin (PV; 7.7 ± 0.8%) subtypes representing the majority of co–labeled cells, as reported previously[8,9,10]. Other GABAergic subtypes examined included: calretinin (CR; 6.4 ± 1.3%), neuropeptide Y (NPY; 7.5 ± 1.1%), reelin (12.5 ± 1.5%), and vasoactive intestinal peptide (VIP; 0%). None of the MGE–GFP cells expressed CamKII (excitatory neurons) or doublecortin (immature neurons). A small percentage of cells around the injection site co–labeled for olig2 (oligodendrocytes; 1.8%) or glial fibrillary acid protein (GFAP; astrocytes; 1%) and failed to exhibit neuronal electrophysiological properties (Supplementary Fig. 3). Similar results were also obtained using adult epileptic mice as recipients, indicating that dispersion or marker expression of the transplanted cells was not affected in epileptic mice (Fig. 1c, d).

Next, we examined the electrophysiological and molecular properties of MGE–GFP neurons using visualized patch–clamp recordings in combination with *post hoc* single–cell RT–PCR. In acute hippocampal slices from transplanted animals (60–65 DAT), MGE–GFP cells exhibited electrophysiological phenotypes and RNA expression profiles consistent with mature interneurons of a MGE lineage[21] (Fig. 2; Supplementary Table 2).

Electrophysiological recordings from 46 cells revealed four main subtypes of interneurons: (i) fast–spiking (n=12; 26%), (ii) regular–spiking non–pyramidal (n=19; 41%), (iii) late–spiking (n=4; 9%), and (iv) burst–spiking (n=11; 24%). All interneurons examined for RNA transcript (n=9) expressed *Lhx6*, a transcription factor marking MGE–derived interneurons, and other gene markers expressed in MGE–derived GABA neurons (Fig. 2a–g). None of the recorded cells contained RNA for the ionotropic serotonin receptor, 5HT3A, or VIP, which are expressed in cortical interneurons from the caudal ganglionic eminence[21]. Voltage–clamp recordings confirmed the presence of spontaneous excitatory postsynaptic currents in all grafted interneurons (Fig. 2i, j; Supplementary Table 3), consistent with functional integration of these cells into the hippocampal network. Taken together, these findings indicate that the adult hippocampus is permissive for migration and functional integration of embryonic GABA progenitors and that these cells differentiate into mature interneurons.

To test the effect of transplanted MGE cells on spontaneous seizures, we performed continuous video–EEG monitoring in the pilocarpine model[18,19]. After an acute episode of pilocarpine–induced status epilepticus in P51 adult mice, animals were first video monitored for 9–20 days to document the emergence of at least one spontaneous seizure before random assignment into untreated, vehicle–injected, or MGE–injected groups (Supplementary Fig. 1). After seizure confirmation, we made bilateral injections of MGE cells into hippocampus (four injections of $3 \times 10^4$ cells per hippocampi). This approach distributed newly generated inhibitory neurons throughout the adult hippocampus of epileptic recipients at 60+ DAT (Fig. 3). In a separate group of animals, we made bilateral injections into basolateral

amygdala (a single injection of $3 \times 10^4$ cells per hemisphere); dispersion and marker expression of MGE cell grafts into the amygdala were comparable to hippocampus (Fig. 4). We chose these brain regions, because they exhibit significant neuropathology[1,2,15,22], including inhibitory neuron loss, and contribute to seizure generation in this model[1,2,17].

All untreated (n=7) or vehicle–injected (n=7) epileptic animals displayed spontaneous electrographic seizures (Fig. 5a), consisting of high–frequency, high–voltage, rhythmic activity with clear onset and termination and prominent voltage spikes preceding ictal events (frequency: 2.36 ± 0.46 seizures per day, n=14). Electrographic seizures or high–voltage spiking were never observed in naïve controls that did not receive pilocarpine (n=3). Simultaneous video monitoring confirmed convulsive, Racine stage 3–5 seizure behaviors during electrographic events[23] (Supplementary Movie 1). Epileptic animals that received injections of MGE cells into the hippocampus exhibited a 92% reduction in seizure frequency (frequency: 0.17 ± 0.09; n=8; Fig. 5b). In 50% of these mice no electrographic seizures were observed during the entire video–EEG monitoring period (7–10 d). In contrast, transplantation into the basolateral amygdala had no effect on seizure frequency (frequency: 2.24 ± 0.46, n=8). The duration of electrographic events or behavioral severity was not different in MGE–grafted animals compared with untreated or vehicle–injected epileptic animals (Supplementary Table 4).

We next asked whether MGE cell transplantation affected mossy fiber sprouting into the inner molecular layer of the dentate gyrus, a well–characterized pathology in epilepsy patients and animal models[1,2,15,24]. To visualize mossy fibers, we stained for zinc transporter 3 (ZnT3), which is highly expressed in mossy fiber terminals[25] (Supplementary Fig. 4). Robust mossy fiber sprouting was present in all vehicle–injected epileptic animals (Timm Score= 2.85 ± 0.1; n=4) and 60 DAT in mice that received MGE cell grafts into the hippocampus (Timm Score= 2.75 ± 0.13; n=4), but not controls (Timm Score= 0; n=4). One–way ANOVA on ranks analysis showed that Timm scores for mossy fiber sprouting were not significantly different between vehicle–injected epileptic animals and mice that received MGE cell grafts ($H = 8.045$; Tukey's *post–hoc*; $P > 0.05$), but both groups had significantly greater Timm scores compared to controls ($P < 0.05$). This observation suggests that the dramatic decrease in seizures obtained with MGE cell transplantation was not due to a reversal of abnormal mossy fiber sprouting in the dentate gyrus.

Quality of life in epilepsy patients is often profoundly impacted by cognitive decline, and epilepsy can be accompanied by debilitating neurobehavioral comorbidities including psychiatric disorders, anxiety, or social problems[26]. Therefore, we examined whether MGE cell transplantation could rescue any of the well–characterized behavioral phenotypes associated with the pilocarpine model[18]. A handling test showed that epileptic mice had a profound increase in their reaction to handling. All epileptic mice displayed aggressive behaviors to touch, which were rare in controls. MGE cell transplantation into hippocampus rescued this abnormal behavior to control levels, but transplantation into amygdala had no effect (Fig. 6a; Supplementary Movie 2). During a 10 min open field test (locomotion), epileptic mice displayed hyperactivity and traveled significantly farther than controls. This behavioral deficit was reversed by cell transplantation into the hippocampus or amygdala (Fig. 6b). In an accelerating rotarod assay (motor coordination), we did not observe a

significant difference among treatment groups in either r.p.m. reached or amount of time spent on the rod (Fig. 6c, d). In the elevated plus maze (general anxiety), differences among treatment groups were not found in either number of open or closed arm entries or amount of time spent in the open arms (Fig. 6e, f). In the forced swim test (despair), control mice developed a characteristic immobile posture when placed into a water–filled cylinder from which they could not escape, but most epileptic mice continued to swim, trying to escape the cylinder throughout the test duration. MGE transplantation into the hippocampus or amygdala of epileptic animals did not alter this behavior (Fig. 6g).

Finally, we asked whether MGE cell transplantation affected performance in a Morris water maze test, which requires the use of external visual cues to locate a hidden platform and escape the water. Mice were first examined on their ability to locate a visible platform (cued learning) and then to locate a hidden platform (acquisition). Then, the hidden platform was removed (probe trial) to measure the short–term retention of spatial memory. Nearly all mice showed improvement in time to find a visible platform, demonstrating efficient cued learning (Fig. 6h); two mice in the “epilepsy” group and 1 mouse that received MGE cell grafts into amygdala were excluded from further analysis because they showed a significant deficit in the visible platform training (Supplementary Figure 5), which can confound the interpretation of spatial learning deficits in the hidden platform task[27,28]. During a hidden platform test (Fig 6i), epileptic animals that did not receive MGE cell grafts had significantly longer escape latencies compared to controls, consistent with previous reports and impaired spatial learning[18,27,28], although the possibility that non–cognitive deficits might influence water maze performance in these animals cannot be excluded. This deficit was confirmed in a probe test 1hr following the final testing session (Fig 6j–l). Whereas controls spent significantly more time in the target quadrant and made numerous platform crossings, epileptic animals showed no preference for any quadrant and rarely crossed the platform location. MGE cell transplantation into hippocampus rescued these deficits in escape latencies, quadrant time, and platform crossings to control levels. However, mice that received MGE cell grafts into amygdala did not show improvement in spatial learning and were indistinguishable from untreated epileptic animals.

## Discussion

Our results show that MGE progenitor cells grafted into the adult epileptic brain exert a significant therapeutic effect on seizures and abnormal behaviors commonly associated with epilepsy. The degree to which this procedure was successful in abrogating seizures in the pilocarpine model is remarkable given that neuropathology (e.g., mossy fiber sprouting) due to pre–existing limbic epilepsy remains present in these animals and the reported difficulty of controlling spontaneous seizures using conventional antiepileptic treatments[19]. Improved behavior after MGE cell grafting into epileptic animals could be relevant to other brain disorders that involve a disruption of inhibitory circuits in hippocampus, such as Alzheimer’s disease[29] or autism[4]. Not surprisingly, these neurological disorders often involve increased seizure susceptibility as a co–morbidity. Interneuron–based cell transplantation might have an important clinical advantage over current therapeutic approaches in that cell grafts can be targeted to spatially restricted brain regions as a one–time procedure for seizure control. In addition to obvious benefits for promoting functional

recovery, this approach might also be useful for limiting adverse behavioral side effects that can be associated with medications or for sparing areas of the epileptic brain normally targeted for surgical resection.

Although our goal was not to examine the site of seizure initiation in this epilepsy model, we did find that interneuron cell grafts into hippocampus, but not amygdala, was critical for controlling epileptic activity. Despite the potentially widespread tissue damage associated with systemic pilocarpine administration[1,2,12,19], these findings are consistent with reports that around 70% of electrographic seizure events can originate within the hippocampal formation in this model[14]. Our findings support a critical role for the loss of inhibitory neurons in epilepsy, a pathology that likely contributes to reduced synaptic inhibition observed in the hippocampus of epileptic pilocarpine–treated rodents[30–32]. Enhancement of GABA–mediated synaptic inhibition that is associated with new MGE–derived interneurons[12–14,33] further supports the concept that abnormal electrical activity is kept in check by a powerful interneuron–mediated “inhibitory restraint”[34–36] and that this enhancement may be sufficient to prevent seizure initiation. Given that we assessed animals around 80–100 days after the induction of status epilepticus, a time when epilepsy is well established in this model, it also seems reasonable to conclude that GABA progenitor cell transplantation has long–term effects on seizures and behavior.

A major challenge in the field has been to develop new approaches for controlling epilepsies that do not respond to current medications. Our results show that GABA progenitors are particularly promising candidates for cell therapy, because they can be broadly distributed within spatially restricted brain regions in adult behaving animals. This approach is based on the functional engraftment of new inhibitory interneurons into existing circuits, and in contrast to optogenetic–[6,7] or stimulation–[37] based approaches, does not require a system for real–time seizure detection. Although production of a comparable and safe MGE–like human stem cell line will ultimately be necessary before translation to the clinic, our results are an encouraging step toward utilizing inhibitory neurons for brain repair in adults with severe forms of epilepsy.

## Online Methods

### Animals

Mice were maintained in standard housing conditions on a 12h light/dark cycle with food and water provided *ad libitum*. All protocols and procedures followed the guidelines of the Laboratory Animal Resource Center at the University of California, San Francisco. Young adult CD1 mice used for pilocarpine injections and breeding were purchased from Charles River Laboratories. Embryonic donor tissue was produced by crossing wild–type CD1 mice to homozygous β–actin:GFP mice. Pilocarpine injections (289 mg/kg) were performed in adult P51 male mice as described previously[15]. After recovering from acute status epilepticus, mice were housed singly and monitored for chronic spontaneous seizures between 9 and 20 days after pilocarpine administration by video recording. Animals only became candidates for transplantation after motor seizures of grade 3 or greater were detected, according to a modified Racine rating scale[15,23]. Animals that were not observed to have spontaneous seizures were euthanized around 25 days after pilocarpine injection.

### Tissue dissection and transplantation

Ventricular and subventricular layers of the MGE were harvested from E13.5 β–actin:GFP embryos. The time point when the sperm plug was detected was considered E0.5. Embryonic MGE explants were dissected in Leibovitz L–15 medium, mechanically dissociated by repeated pipetting in medium containing DNase I (100 μg $ml^{-1}$), and then concentrated by centrifugation (2 min at 1,000 × g). Concentrated cell suspensions (~$10^3$ cells $nl^{-1}$) were front loaded into bevelled glass micropipettes (40–50μm tip diameter; Wiretol 5 μl; Drummond Scientific Company) and injected ($3 \times 10^4$ cells per injection) into the hippocampus or amygdala of adult control or epileptic CD1 mice (P60 to P76). All injection coordinates were first verified in a series of preliminary dye and/or cell injection studies into control and epileptic mice (Supplementary Figure 6). For hippocampal transplantations, injections were made into stratum radiatum of the CA3 subfield at the following stereotaxic coordinates (in mm): antierior–posterior (AP) 1.75, medial–lateral (ML) 2.3, dorsal–ventral (DV) 1.7. A second group of injections were made at three sites along the length of the hippocampus (in mm): AP 3.25, ML 3.0, and DV 3.65, 2.9, and 2.0. For amygdala transplantations, injections were made into the basolateral nuclei at the following coordinates (in mm): AP 1.5, ML 3.65, and DV 3.7. Sham–operated controls were injected with an equal volume of vehicle at each site (i.e., 4 sites per hemisphere for hippocampus, one site per hemisphere for amygdala). For migration studies, only a single injection was made into the right, dorsal CA3 region of the hippocampus. For behavior and EEG experiments, transplantations were only considered successful if the density and migration of GFP cells in the recipient brain were evenly distributed in both hemispheres and confirmed as ≥30,000 cells (hippocampus; range: 34,200 to 68,100) or ≥5,000 cells (amygdala; range: 5,800 to 8,600) per animal and ≥600 μm from the injection site; these criteria were met in all mice. Cell viability (74.1 ± 1.7%) and concentration were quantified using 0.5 μl of the cell suspension mixed with 24.5 μl of L–15 medium and 25 μl of Trypan Blue (Sigma) as described previously[38].

### Immunostaining

Mice were transcardially perfused with 4% paraformaldehyde and free–floating vibratome sections (50 μm) were processed using standard immunostaining procedures (12–14). Primary antibodies and dilutions are provided in Supplementary Table 1. For ZnT3 staining, we used a TSA™ Cyanine 3 System kit (Perkin Elmer; product no. NEL704A001KT) for signal amplification. Secondary antibodies were: Alexa 488 and Alexa 594 (Invitrogen). Sections were then mounted on charged slides (Superfrost plus; Fisher Scientific) with Vectasheild that contained DAPI. Images were obtained with a spinning disk confocal microscope (Nikon Yokogawa CSU–X1 Borealis). Epiflourescent images were obtained using a Nikon Eclipse microscope. Brightness and contrast were adjusted manually using Adobe Photoshop.

### Cell quantification

Transplanted GFP–labeled cells were directly counted in fluorescently labeled sections (50 μm) from recipient animals as described previously[12–14]. All transplanted cells that expressed GFP were counted in every sixth coronal section in all layers of the entire

hippocampus or amygdala (i.e., 300 μm apart) using a Nikon Eclipse microscope with an x40 objective.

## Electrophysiology

Coronal brain slices (300 μm thickness) were prepared from recipient mice 60–65 DAT. Slices were submerged in the recording chamber and continuously perfused with oxygenated ACSF (32 –34°C) containing (in mM): 124 NaCl, 3 KCl, 1.25 $NaH_2PO_4$–$H_2O$, 2 $MgSO_4$–$7H_2O$, 26 $NaHCO_3$, 10 dextrose, and 2 $CaCl_2$ (pH 7.2–7.4, 300–305 mOsm/kg). Whole–cell patch–clamp recordings from GFP–labeled cells were performed at x40 using an upright, fixed–stage microscope (Olympus BX50WI) equipped with infrared, differential interference contrast (IR–DIC) and epifluorescence optics. Patch pipettes (3–5 MΩ) were filled with an internal solution, containing (in mM): 140 $K^+$ gluconate, 1 NaCl, 5 EGTA, 10 HEPES, 1 $MgCl_2$, 1 $CaCl_2$, 3 KOH, 2 ATP, and 0.2% biocytin, pH 7.21. Recordings were obtained with an Axopatch 1D amplifier, filtered at 5 kHz, and recorded to pClamp 10.2 software (Clampfit; Axon Instruments). Spontaneous EPSCs were examined at a holding potential of −70 mV. Series resistance was typically <15 MΩ and was monitored throughout the recordings. Data were only used for analysis if the series resistance remained <20 MΩ and changed by ≤20% during the recordings. Recordings were not corrected for a liquid junction potential. Resting membrane potentials were measured immediately after breakthrough by temporarily removing the voltage clamp and monitoring voltage. For current–clamp recordings, cells were held at −70 mV, and electrophysiological properties were measured in response to a series of long (1000 ms) hyperpolarizing and depolarizing current–injections (10 pA steps; range: −80 pA to 1000 pA). Data analysis was performed using pClamp 10.2 (Clampfit, Axon Instruments), MiniAnalysis 6.0 (Synaptosoft), Microsoft excel, and Sigmaplot 12.3 programs. A 2 min sample recording per cell was used for measuring EPSC characteristics. Events characterized by a typical fast rising phase and exponential decay phase were manually detected using MiniAnalysis. The threshold for event detection was currents with amplitudes greater than three times the root mean square (RMS) noise level.

## Single–cell RT–PCR

At the end of the recording session (<15min), the cytoplasm of the cell was aspirated into the recording pipette while maintaining a tight seal similar to the method described previously[21]. The pipette was carefully removed and its contents (~6 μl) expelled into a test tube containing 1.5μl nuclease free water and 1μl RNaseOUT (40 U $\mu l^{-1}$) and stored at −80°C. Samples were incubated with DNase I (Invitrogen) according to manufacturer instructions for complete removal of genomic DNA. Reverse transcription (RT) was then performed using 2μl 10x RT buffer, 1μl mixed 10mM deoxy NTPs, 4μl 25mM $MgCl^2$, 2μl 0.1M DTT, 1μl random hexamer (50 ng $\mu l^{-1}$), and 1μl SuperScript III RT (Invitrogen) in a final volume of 22μl. Next, two consecutive rounds of PCR were performed using outer and nested primer pairs[21,39] (Supplementary Table 2). All targets were first amplified simultaneously using 1μl of each primer (20 pmol $\mu l^{-1}$) and 40μl 2x GoTaq Green Master Mix in a final volume of 100μl. Targets were amplified using 5 min of initial denaturation at 94°C followed by 21 cycles of denaturing at 94°C for 30s, annealing at 60°C for 30s, elongation at 72°C for 35s, and 7min of final elongation at 72°C. Next, individual targets

were reamplified separately for 20 cycles of PCR with the same thermal cycling conditions using 3μl of the first PCR product as a template and nested primer sets. Products were assayed on a 1.5% agarose gel stained with ethidium bromide, using a 100bp DNA ladder (Thermo Scientific) as a molecular weight marker. All primer sets were first verified on 1 ng of total RNA purified from GFP mouse hippocampus using the RT–PCR protocol described above (n=2; Fig 2f; see Supplementary Table 2 for predicted sizes of PCR–generated fragments). To rule out mRNA contamination from surrounding tissue, patch pipettes were placed into the slice without seal formation, and after the removal of the pipette, its content was processed as described above (*n*=3). To rule out contamination of reaction materials, PCR was performed using nuclease free water in place of a sample (n=5). No PCR product was obtained using these protocols.

### Video–EEG

EEG recordings were obtained using a time–locked video EEG monitoring system (Pinnacle Technologies). Each mouse was anesthetized with ketamine and xylazine (10 mg/kg and 1 mg/kg i.p.) so that there was no limb–withdrawal response to a noxious foot pinch. Sterile, stainless steel bone screw recording electrodes were placed epidurally through burr holes in the skull (one electrode on either side of the sagittal suture, approximately halfway between bregman and lambdoid sutures and ≈1 mm from the midline) using surface head–mount EEG hardware (Pinnacle Technologies). Electrodes were cemented in place with a fast–acting adhesive and dental acrylic. Two wires were laid on the shoulder muscles for electromyographic (EMG) recording. Animals were allowed to recover for 3 days before experiments were initiated. Electrographic seizures were defined as high–frequency, high voltage synchronized polyspike or paroxysmal sharp waves with amplitude >2–fold background that lasted ≥15 sec. Electrographic EEG seizures were analyzed by two investigators who were blinded to the treatment condition of the animals using SireniaScore software (Pinnacle) and confirmed by offline review of behavioral video recordings obtained at two different viewing angles. Behaviors were scored according to a modified Racine rating scale (12, 20). Experimental animals were monitored for 7–10 days (24 h/day). Because electrographic seizure characteristics in untreated and vehicle–injected epileptic mice were comparable in frequency (2.8 ± 0.5 seizures per day vs. 1.9 ± 0.4 seizures per day; $P$ =0.3, two–tailed t–test) and duration (54.4 ± 2.8 s vs. 56.0 ± 3.1 s; $P$ =0.8, two–tailed t–test), the data from these groups were pooled. A total of 24 days of recording were analyzed for control mice ($n$ = 3), 111 days for untreated or vehicle–treated epileptic mice ($n$ =14), 64 days for mice that received MGE cell grafts into the hippocampus ($n$ = 8), and 65 days for mice that received MGE cell grafts into the amygdala ($n$ = 8).

### Behavior

All behavioral testing was conducted during the light phase of the light/dark cycle under the guidance and supervision of the UCSF Neurobehavioral Core for Rehabilitation Research (NCRR) facility. Pilocarpine–injected mice and age–matched controls were housed singly starting immediately after the induction of status epilepticus. Mice were tested in two separate groups in the following order: Group 1, open field test (before pilocarpine injections), open field test (14 d after pilocarpine injections), handling test around 60 DAT, open field test ~24h after the handling test, rotarod immediately following the final open

field session and then 2–3 d later, EEG surgery and monitoring; Group 2 (60 DAT): elevated plus maze, Morris water maze, and forced swim test. Animal identities were coded, and all behaviors were performed and analyzed by two investigators who were blinded to the treatment condition of the animals.

### Open field test

Mice were placed in the center of a 40 cm × 40 cm × 38 cm SmartFrame open field arena (Kinder Scientific) for 10 min under standard overhead lighting conditions. Behavioral performance was recorded using a computer–operated tracking system (MotorMonitor, Kinder Scientific).

### Rotarod

Mice were placed on a rotarod apparatus (UGO–Basile, model 7650) that accelerated from 4 to 40 rpm over 3.5 min and then maintained at 40 rpm for another 1.5 min. All animals were first acclimated to the rotarod immediately following the final open field testing session and then tested 2–3 d later. Performance was assessed by measuring the latency until the mouse fell completely off the rod or gripped the device and spun around without attempting to walk on the rod. Three trials were performed and both the rpm reached and total time spent on the rod were averaged across the trials for each mouse.

### Handling Test

Reaction to handling was assessed using a semiquantitative handling test described previously[40]. The test included four measures: (i) “nonstressful” handling was performed by rubbing slowly along the back of the mouse in a petting motion in the direction of the grain of fur with a latex–gloved hand, (ii) “stressful” handling was performed by rubbing vigorously against the grain of fur, (iii) pinching at the tail tip with a plastic–tipped hemostat, and (iv) pinching at the tail base. Each task was performed for 15 seconds. Reaction to handling was scored for each task using a four–point rating scale: 1, initial struggle but calmed within 15 seconds; 2, struggle for more than 15 seconds; 3, struggle for more than 15 seconds and exhibited one or more defensive reactions (piloerection, flattening of the ears against the head, attempt to bite or back away from the experimenter); and 4, struggled for more than 15 seconds and exhibited flight behavior (loud vocalization or wild running).

### Elevated plus maze

The elevated plus maze apparatus (Kinder Scientific) was comprised of two open arms (38 × 2 cm) and two enclosed arms (38 × 2 × 15 cm), elevated 64 cm above the floor level. Mice were placed in the central platform always facing the same open arm. Test duration was 5 min under standard overhead lighting conditions. All data were collected using Ethovision software (Noldus Information Technology).

### Morris water maze

The Morris water maze task was conducted similar to the method described previously[28,41]. A white, circular pool (140 cm in diameter) was filled with water (22–24°C) that was mixed

with black, nontoxic paint to make it opaque, and a circular platform (15 cm in diameter) was submerged 1 cm beneath the surface of the water. The testing room was filled with a number of visual cues. Mice were first trained to locate a visible platform (days 1 and 2) and then a submerged hidden platform (days 3–5) in two daily sessions ~3.5 hr apart. Each session consisted of three 60 s trials with an intertrial interval of 310–15 min. Mice were allowed to swim until they found the platform, and if they did not find the platform within 60 s, they were guided to it by the experimenter. During visible platform training, the platform was moved to a new, random location quadrant for each session, and mice were placed in a different starting location for each trial. Exclusion criteria for visible platform performance were defined as an average latency (mean of all trials in sessions 3 and 4) greater than the average escape latency plus two SD in naïve controls[28]. During the hidden platform task, mice were placed in a different starting location for each trial, but the platform remained in the same location for each trial (in the center of the target quadrant). Time to reach the platform, path length, and swim speed were recorded with a video tracking system (Noldus Information Technology). Because there were no significant differences in average swim speeds between the treatment groups during the visible platform sessions (data not shown), the time required to locate the platform (escape latency) was used as the main measure for analysis. A probe trial was conducted 1h after the final hidden platform testing session; the platform was removed, and mice were placed in the pool and allowed to swim for 60 s.

### Forced swim test

The mouse forced swim test was conducted similar to the method described previously[42]. Mice were placed individually into glass cylinders (height 40 cm, diameter 15 cm) containing 22 cm of water, (22–23 °C) for 6 min. The total duration of immobility was recorded during the last 4 min of the 6 min testing period. A mouse was considered to be immobile when it floated in an upright position, and made only minimal movements to keep its head above water. Trials were video recorded and scored offline by an investigator blinded to the experimental outcome of each animal.

### Statistical analysis

All analyses were performed with SigmaPlot 12.3 software and assessed for normality (Shapiro–Wilk) and variance. Data were compared by t-test, one–way ANOVA for multiple comparisons, nonparametric one–way ANOVA on ranks, or by two–way repeated measures ANOVA. A Tukey's *post hoc* test was performed when appropriate. Sample sizes for behaviors significantly affected by MGE treatment were determined based on Power Analysis, as indicated in Supplementary Table 4. Data are expressed as mean ± standard error (S.E.M.) and significance was set at $P<0.05$.

## Supplementary Material

Refer to Web version on PubMed Central for supplementary material.

## Acknowledgments

This work was supported by funding from National Institutes of Health grants NINDS RO1–NS071785 (S.C.B., J.L.R., and A.A.B.), NINDS F32–NS077747 (R.F.H.), and the California Institute of Regenerative Medicine (CIRM) grant #TR2-01749 (A.A.B and S.C.B.). We thank Matthew Dinday and William Hindle–Katel for assistance with pilocarpine injections, Joy Sebe for tissue dissection training, Gabriella Hortopan for advice on the single–cell RT–PCR procedure, and Sandra Canchola for training on behavior assays.

## References

1. Lothman EW, Bertram EH III, Stringer JL. Functional anatomy of hippocampal seizures. Prog Neurobiol. 1991; 37:1–82. [PubMed: 1947175]
2. [Accessed November, 2012] Jasper's Basic Mechanisms of the Epilepsies—NCBI Bookshelf. http://www.ncbi.nlm.nih.gov/books/NBK50785/
3. Andrews-Zwelling Y, Gillespie AK, Kravitz AV, Nelson AB, Devidze N, Lo I, Yoon SY, Bien-Ly N, Ring K, Zwilling D, Potter GB, Rubenstein JLR, Kreitzer AC, Huang Y. Hilar GABAergic interneuron activity controls spatial learning and memory retrieval. PLoS One. 2012; 7:e40555. [PubMed: 22792368]
4. Han S, Tai C, Westenbroek RE, Yu FH, Cheah CS, Potter GB, Rubenstein JL, Scheuer T, de la Iglesia HO, Catterall WA. Autistic-like behavior in Scn1a+/− mice and rescue by enhanced GABA-mediated neurotransmission. Nature. 2012; 489:385–90. [PubMed: 22914087]
5. World Health Organization. [Accessed January, 2013] Epilepsy, Epilepsy Fact Sheet. http://www.who.int/mediacentre/factsheets/fs999/en/index.html
6. Paz JT, Davidson TL, Frechette ES, Delord B, Parada I, Peng K, Deisseroth K, Huguenard JR. Closed-loop optogenetic control of thalamus as a tool for interrupting seizures after cortical injury. Nat Neurosci. 2012; 16:64–70. [PubMed: 23143518]
7. Krook-Magnuson E, Armstrong C, Oijala M, Soltesz I. On-demand optogenetic control of spontaneous seizures in temporal lobe epilepsy. Nat Commun. 2013; 4:1376. [PubMed: 23340416]
8. Lavadas AA, Grigoriou M, Pachnis V, Parnavelas JG. The medial ganglionic eminence gives rise to a population of early neurons in the developing cerebral cortex. 1999; 19:7881–7888.
9. Wichterle H, Garcia-Verdugo JM, Herrera DG, Alvarez-Buylla A. Young neurons from medial ganglionic eminence disperse in adult and embryonic brain. Nat Neurosci. 1999; 2:461–466. [PubMed: 10321251]
10. Xu Q, Cobos I, De La Cruz E, Rubenstein JL, Anderson SA. Origins of cortical interneuron subtypes. J Neurosci. 2004; 24:2612–22. [PubMed: 15028753]
11. Butt SJ, Fuccillo M, Nery S, Noctor S, Kriegstein A, Corbin JG, Fishell G. The temporal and spatial origins of cortical interneurons predict their physiological subtype. Neuron. 2005; 48:591–604. [PubMed: 16301176]
12. Alvarez-Dolado M, Calcagnotto ME, Karkar KM, Southwell DG, Jones-Davis DM, Estrada RC, Rubenstein JL, Alvarez-Buylla A, Baraban SC. Cortical inhibition modified by embryonic neural precursors grafted into the postnatal brain. J Neurosci. 2006; 26:7380–7389. [PubMed: 16837585]
13. Baraban SC, Southwell DG, Estrada RC, Jones DL, Sebe JY, Alfaro-Cervello C, García-Verdugo JM, Rubenstein JLR, Alvarez-Buylla A. Reduction of seizures by transplantation of cortical GABAergic interneuron precursors into Kv1.1 mutant mice. Proc Natl Acad Sci USA. 2009; 106:15472–15477. [PubMed: 19706400]
14. Southwell DG, Paredes MF, Galvao RP, Jones DL, Froemke RC, Sebe JY, Alfaro-Cervello C, Tang Y, Garcia-Verdugo JM, Rubenstein JL, Baraban SC, Alvarez-Buylla A. Intrinsically determined cell death of developing cortical interneurons. Nature. 2012; 491:109–113. [PubMed: 23041929]
15. Shibley H, Smith BN. Pilocarpine-induced status epilepticus results in mossy fiber sprouting and spontaneous seizures in C57BL/6 and CD-1 mice. Epilepsy Res. 2002; 49:109–20. [PubMed: 12049799]
16. Goffin K, Nissinen J, Van Laere K, Pitkänen A. Cyclicity of spontaneous recurrent seizures in pilocarpine model of temporal lobe epilepsy in rat. Exp Neurol. 2007; 205:501–5. [PubMed: 17442304]

17. Bortel A, Lévesque M, Biagini G, Gotman J, Avoli M. Convulsive status epilepticus duration as determinant for epileptogenesis and interictal discharge generation in the rat limbic system. Neurobiol Dis. 2010; 40:478–89. [PubMed: 20682341]
18. Grötke I, Hoffmann K, Löscher W. Behavioral alterations in the pilocarpine model of temporal lobe epilepsy in mice. Exp Neurol. 2007; 207:329–349. [PubMed: 17714705]
19. Löscher, W. Strategies for antiepileptogenesis: Antiepileptic drugs versus novel approaches evaluated in post-status epilepticus models of temporal lobe epilepsy. In: Noebels, JL.; Avoli, M.; Rogawski, MA., et al., editors. Jasper's Basic Mechanisms of the Epilepsies [Internet]. 4. Bethesda (MD): National Center for Biotechnology Information, US; 2012.
20. Tamamaki N, Yanagawa Y, Tomioka R, Miyazaki J, Obata K, Kaneko T. Green fluorescent protein expression and colocalization with calretinin, parvalbumin, and somatostatin in the GAD67–GFP knock-in mouse. J Comp Neurol. 2003; 467:60–79. [PubMed: 14574680]
21. Tricoire L, Pelkey KA, Erkkila BE, Jeffries BW, Yuan X, McBain CJ. A blueprint for the spatiotemporal origins of mouse hippocampal interneuron diversity. J Neurosc. 2011; 31:10948–70.
22. Vignoli T, Nehlig A, Massironi SG, de Coimbra RC, da Mazzacoratti MG, Silva IR, Neto EF, Persike DS, Fernandes MJ. Consequences of pilocarpine-induced status epilepticus in immunodeficient mice. Brain Res. 2012; 1450:125–37. [PubMed: 22405727]
23. Racine RJ. Modification of seizure activity by electrical stimulation. II. Motor seizure. Electroencephalogr Clin Neurophysiol. 1972; 32:281–294. [PubMed: 4110397]
24. Babb TL, Kupfer WR, Pretorius JK, Crandall PH, Levesque MF. Synaptic reorganization by mossy fibers in human epileptic fascia dentata. Neuroscience. 1991; 42:351–363. [PubMed: 1716744]
25. Palmiter RD, Cole TB, Quaife CJ, Findley SD. ZnT-3, a putative transporter of zinc into synaptic vesicles. Proc Natl Acad Sci U S A. 1996; 93:14934–9. [PubMed: 8962159]
26. Hermann B, Seidenberg M, Jones J. The neurobehavioural comorbidities of epilepsy: can a natural history be developed. Lancet Neurol. 2008; 7:151–160. [PubMed: 18207113]
27. D'Hooge R, De Deyn PP. Applications of the Morris water maze in the study of learning and memory. Brain Res Rev. 2001; 36:60–90. [PubMed: 11516773]
28. Palop JJ, Jones B, Kekonius L, Chin J, Gui-Qui Y, Raber J, Masliah E, Mucke L. Neuronal depletion of calcium-dependent proteins in the dentate gyrus is tightly linked to Alzheimer's disease-related cognitive deficits. Proc Natl Acad Sci. 2003; 100:9572–77. [PubMed: 12881482]
29. Verret L, Mann EO, Hang GB, Barth AM, Cobos I, Ho K, Devidze N, Masliah E, Kreitzer AC, Mody I, Mucke L, Palop JJ. Inhibitory interneuron deficit links altered network activity and cognitive dysfunction in Alzheimer model. Cell. 149:708–27. [PubMed: 22541439]
30. Hirsch JC, Agassandian C, Merchan-Perez A, Ben-Ari Y, DeFelipe J, Esclapez M, Bernard C. Deficit of quantal release of GABA in experimental models of temporal lobe epilepsy. Nat Neurosci. 1999; 2:499–500. [PubMed: 10448211]
31. Cossart R, Dinocourt C, Hirsch JC, Merchan-Perez A, De Felipe J, Ben-Ari Y, Esclapez M, Bernard C. Dendritic but not somatic GABAergic inhibition is decreased in experimental epilepsy. Nat Neurosci. 2001; 4:52–62. [PubMed: 11135645]
32. Kobayashi M, Buckmaster PS. Reduced inhibition of dentate granule cells in a model of temporal lobe epilepsy. J Neurosci. 2003; 23:2440–52. [PubMed: 12657704]
33. Zipancic I, Calcagnotto ME, Piquer-Gil M, Mello LE, Alvarez-Dolado M. Transplant of GABAergic precursors restores hippocampal inhibitory function in a mouse model of seizure susceptibility. Cell Transplant. 2010; 19:549–64. [PubMed: 20144261]
34. Chagnac-Amitai Y, Connors BW. Horizontal spread of synchronized activity in neocortex and its control by GABA-mediated inhibition. J Neurophysiol. 1989; 61:747–58. [PubMed: 2542471]
35. Trevelyan AJ, Sussillo D, Yuste RM. Feedforward inhibition contributes to the control of the speed of epileptiform propagation. J Neurosci. 2007; 27:3383–3387. [PubMed: 17392454]
36. Schevon CA, Weiss SA, McKhann G Jr, Goodman RR, Yuste R, Emerson RG, Trevelyan AJ. Evidence of an inhibitory restraint of seizure activity in humans. Nat Commun. 2012; 3:1060. [PubMed: 22968706]
37. Berenyi A, Belluscio M, Mao D, Buzsaki G. Closed-loop control of epilepsy by transcranial electrical stimulation. Science. 2012; 337:735–7. [PubMed: 22879515]

38. Marchenko S, Flanagan L. Counting human neural stem cells. J Vis Exp. 2007; (7):e262.10.3791/262

39. Vucurovic K, Gallopin T, Ferezou I, Rancillac A, Chameau P, van Hooft JA, Geoffroy H, Monyer H, Rossier J, Vitalis T. Serotonin 3A receptor subtype as an early and protracted marker of cortical interneuron subpopulations. Cereb Cortex. 2010; 20:2333–47. [PubMed: 20083553]

40. Mortazavi F, Ericson M, Story D, Hulce VD, Dunbar GL. Spatial learning deficits and emotional impairments in pentylenetetrazole-kindled rats. Epilepsy Beh. 2005; 4:629–38.

41. Raber J, Bongers G, LeFevour A, Buttini M, Mucke L. Androgens protect against apilipoprotein E4-induced cognitive deficits. J Neurosci. 2002; 22:5204–09. [PubMed: 12077215]

42. Can A, Dao DT, Arad M, Terrillion CE, Piantadosi SC, Gould TD. The Mouse Forced Swim Test. J Vis Exp. 2012; (59):e3638.10.3791/3638 [PubMed: 22314943]

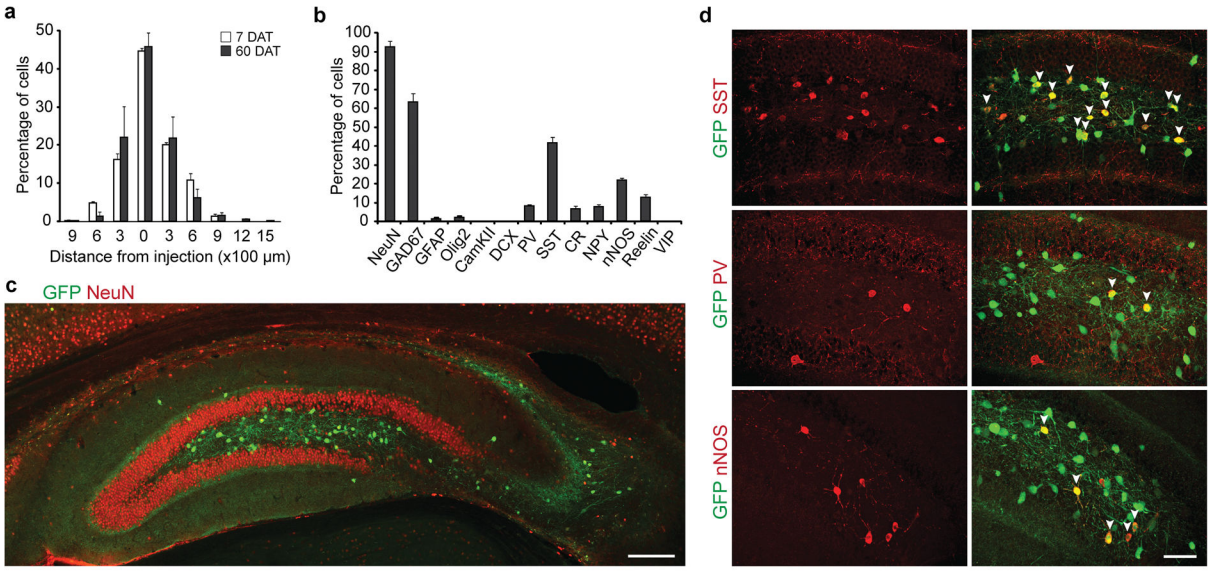


**Figure 1. Transplanted MGE cells migrate into the adult hippocampus and express markers of inhibitory neurons**

**a.** Distribution of transplanted E13.5 MGE cells expressing GFP under β–actin promoter 7 DAT (white bars, n=3 animals) and 60 DAT (grey bars; n=6 animals). **b.** Quantification of marker expression in GFP–labeled cells (n=3–6 animals per marker). **c.** Hippocampus of a pilocarpine–injected recipient mouse (60 DAT) labeled for NeuN (red) and transplanted GFP–labeled inhibitory neurons (green). Transplanted neurons disperse after grafting into recipient animals despite extensive hippocampal cell loss due to pilocarpine injection. **d.** At 60 DAT, GFP–labeled cells (green) coexpress SST, PV, and nNOS (all in red). White arrowheads identify colabeled cells. Error bars represent SEM. Scale bars: 1000 µm (**c**), 67 µm (**d**).

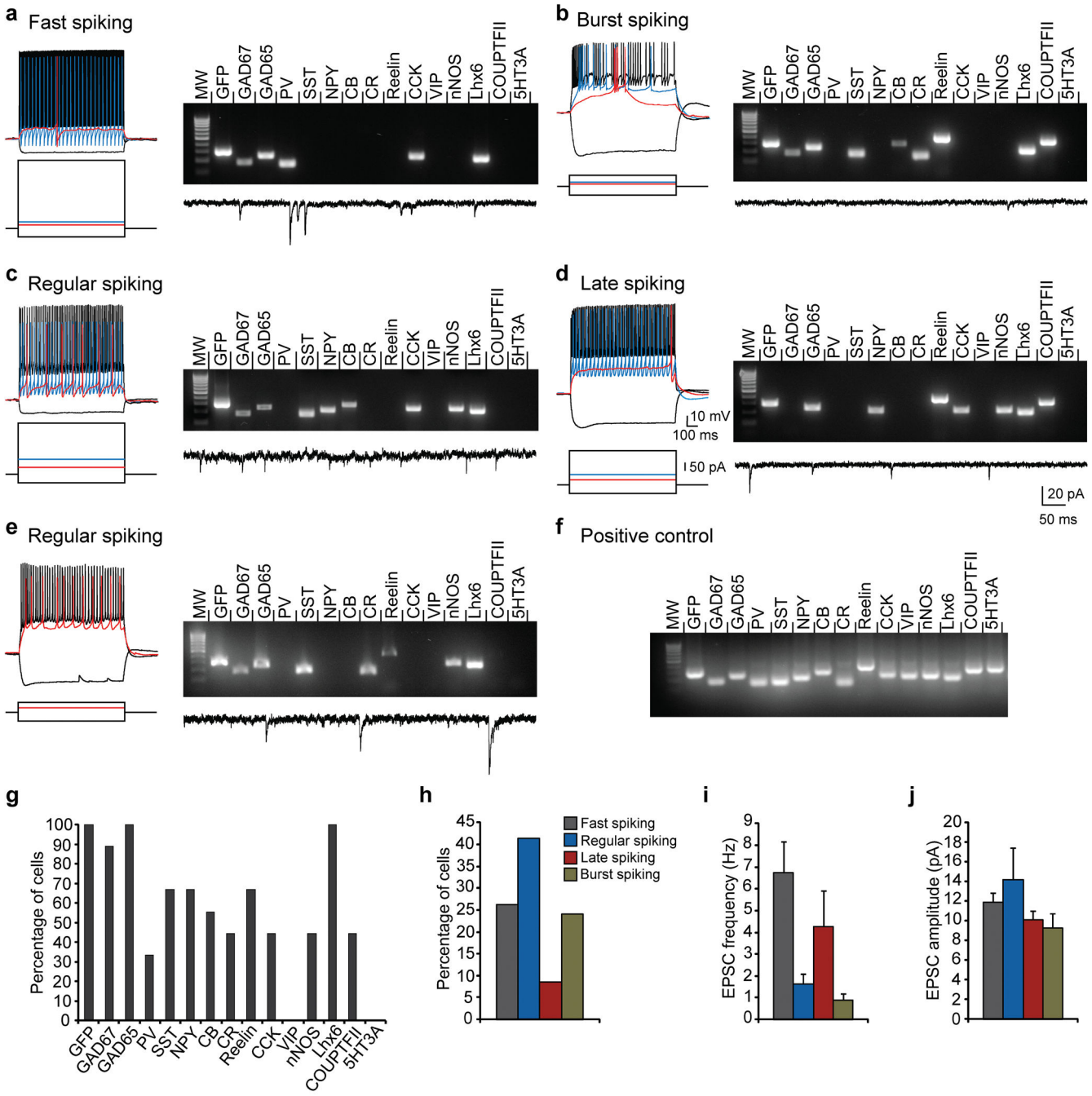


**Figure 2. Transplanted MGE cells differentiate into functional inhibitory interneurons**

**a–e.** Example electrophysiological responses of five different transplanted MGE cells to the indicated square wave current pulses (bottom) from a holding potential near −70mV. Recordings were obtained from slices 61–65 DAT. Depolarizing current pulses and corresponding responses are for near threshold (red), 2x threshold (blue), and near maximal firing (black). Shown at the right are the mRNA profiles obtained from single–cell RT–PCR analysis for each recorded cell. **f.** Positive control for the single–cell RT–PCR procedure using 1ng of hippocampus RNA from a GFP mouse. **g.** Summary plot for the occurrence of

each marker in recorded GFP cells (n=9). RNA was obtained from Regular Spiking (n=3), Fast Spiking (n=2), Burst Spiking (n=3), and Late Spiking (n=1) interneurons. **h.** Occurrence of each interneuron subtype recorded based on firing properties (n=46 cells). **i**, **j.** Mean EPSC frequency (**i**) and amplitude (**j**) according to interneuron subtype. Error bars represent SEM. Electrophysiological properties of grafted interneurons are summarized in Supplementary Table 3.

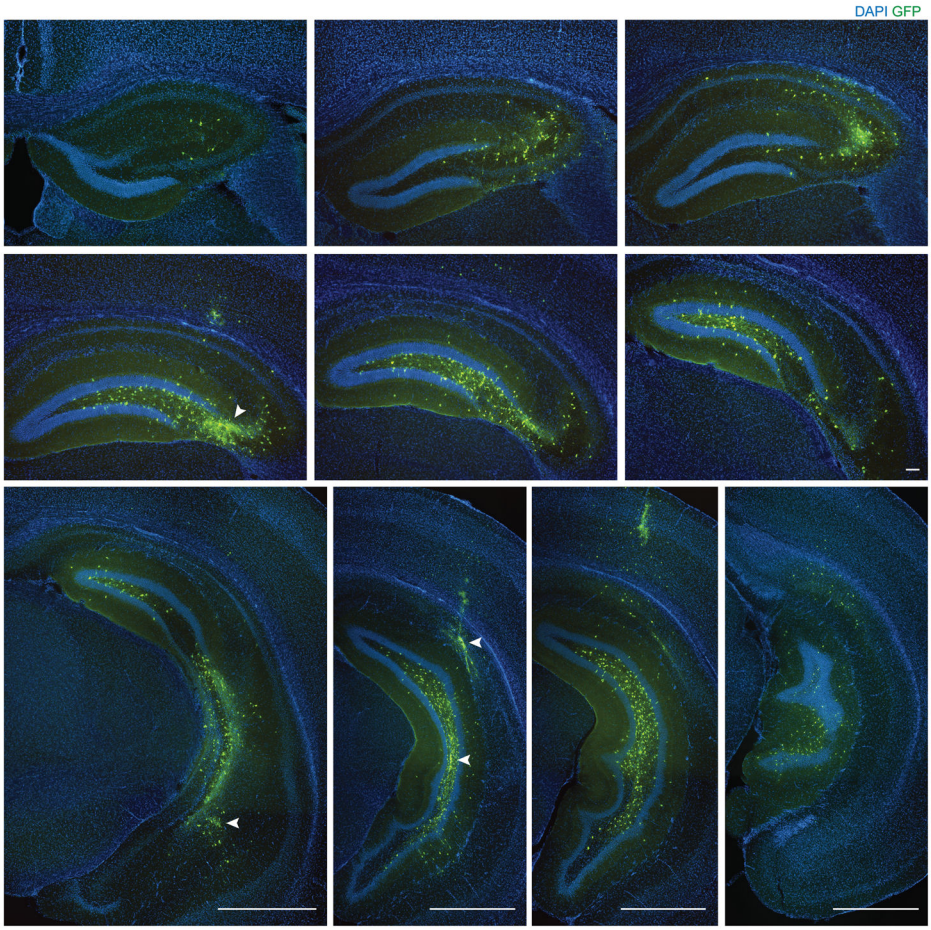


**Figure 3. Distribution of MGE–derived cells 60+ DAT into the adult epileptic hippocampus**

Serial sections (300 μm apart) through the entire hippocampus of a pilocarpine–treated recipient mouse labeled for transplanted MGE cells (green) and DAPI (blue). White arrowheads in **d, g,** and **h** indicate the injection sites. Scale bars: 100 μm (**a–f**), 1000 μm (**g–j**).

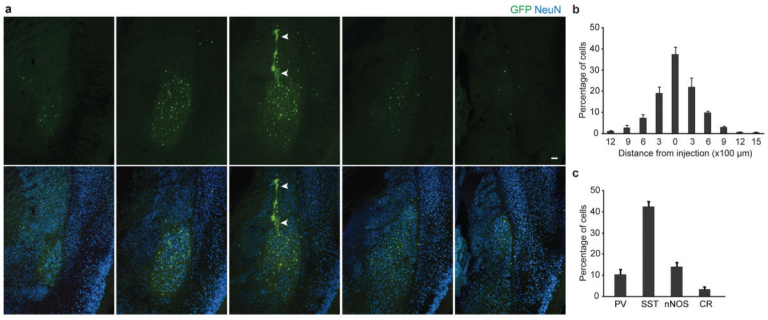


**Figure 4. Distribution of MGE–derived cells 60+ DAT into the adult epileptic amygdala. a** Serial sections (300 µm apart) through the amygdala of a pilocarpine–treated recipient mouse labeled for transplanted MGE cells (green) and NeuN (blue). Cells were found distributed throughout the lateral and basal nuclei, but they were rarely found lateral to the external capsule. White arrowheads indicate the injection tract. Scale bar: 100 µm. **b.** Distribution of transplanted E13.5 MGE cells 60 DAT (n=6 animals). **c.** Quantification of marker expression in GFP–labeled cells (n=3 animals per marker). Error bars represent SEM.

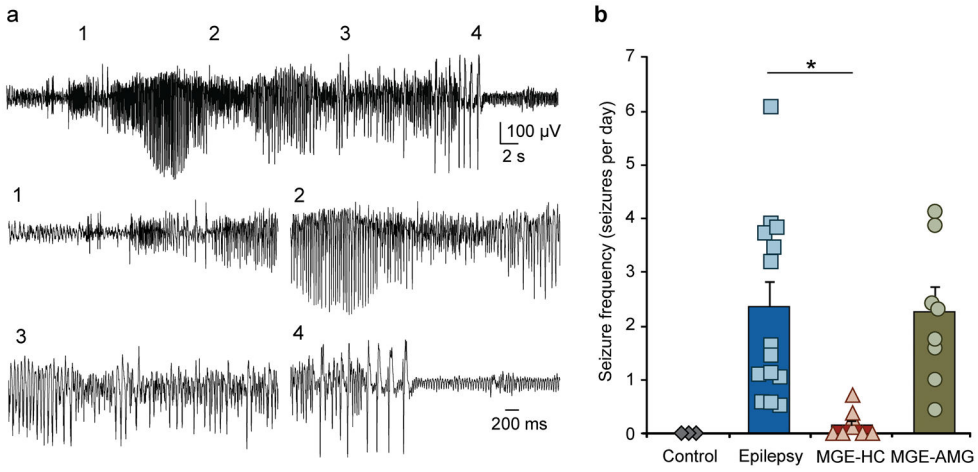


**Figure 5. Inhibitory neuron transplantation reduces seizure occurrence in epileptic animals**

**a.** Example EEG recording of a spontaneous seizure from an untreated epileptic mouse. Numbers indicate regions of the seizure shown below at high resolution. **b**. Bar plots show the mean spontaneous seizure frequency (seizures per day) for each group based on continuous EEG recordings (7–10 d). Bars represent mean ± SEM. The data points superimposed over the bar graph each represent an individual mouse from which recordings were obtained. * $P < 0.01$. Abbreviations: MGE–HC, MGE transplantation into the hippocampus; MGE–AMG, MGE transplantation into the amygdala.

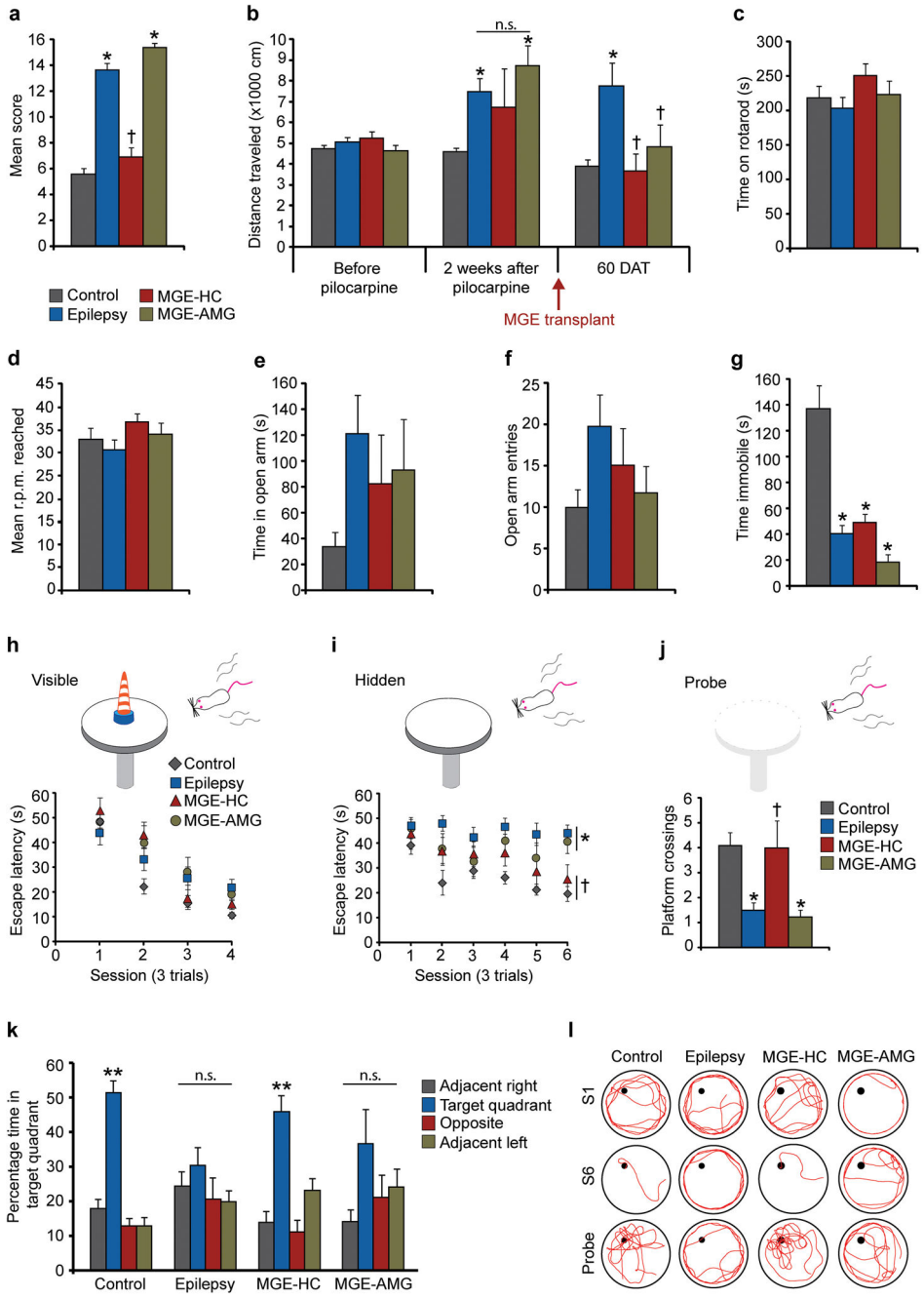


**Figure 6. Inhibitory neuron transplantation rescues behavioral comorbidities of epilepsy**

**a.** Epileptic mice showed an increase in aggressive behaviors to handling compared to naïve controls. This was reversed by MGE cell transplantation into the hippocampus (MGE–HC) but not by transplantation into the amygdala (MGE–AMG). **b.** In the open field test, two weeks after pilocarpine injections mice traveled farther when compared to naïve controls and baseline measurements before pilocarpine injection. MGE cell transplantation into both the hippocampus and amygdala reversed this behavior to control levels, 60 DAT. **c, d.** There was no difference between treatment groups in the amount of time spent on an accelerating

rotarod (**c**) or the mean r.p.m. reached (**d**).**e, f.** In the elevated plus maze, there was no difference between treatment groups in the amount of time spent in the open arm (**e**), or the number of open arm entries (**f**). **g.** In the forced swim test, epileptic mice spent less time immobile compared to controls, and MGE transplantation into the hippocampus or amygdala did not improve this behavior. **h.** In a Morris water maze test, all mice showed a decrease in latency to escape the maze during repeated training trials in the visible platform test. **i.** Epileptic mice showed a profound deficit in latency to escape the maze during the 6 repeated sessions of the hidden platform test. **j, k.** During a probe trial following the final testing session, epileptic mice made fewer platform crossings (**j**) and did not show preference for any quadrant (**k**). MGE cell transplantation into hippocampus, but not transplantation into amygdala, rescued deficits in escape latency (**i**) and probe trial performance (**j, k**) to control levels. **l**. Example locomotion tracking plots show the total path–length during session 1 (S1) and session 6 (S6) of the hidden platform task and the probe trial. A black circle indicates platform location. All data represent mean ± SEM from 7–25 mice per treatment group. * $P < 0.05$ vs control, † $P < 0.05$ vs epilepsy, ** $P < 0.001$ vs other quadrants. All values and statistical analyses are provided in Supplementary Table 4.